



Available online at www.sciencedirect.com

ScienceDirect

Proceedings
of the
Combustion
Institute

Proceedings of the Combustion Institute 38 (2021) 661-669

www.elsevier.com/locate/proci

An extended methodology for automated calculations of non-Boltzmann kinetic sequences: $H + C_2H_2 + X$ and combustion impact

Lei Lei ^a, Michael P. Burke ^{a,b,*}

^a Department of Mechanical Engineering, Columbia University, New York, NY 10027, United States ^b Department of Chemical Engineering, Data Science Institute, Columbia University, New York, NY 10027, United States

Received 8 November 2019; accepted 28 June 2020 Available online 8 October 2020

Abstract

It is generally assumed in phenomenological kinetic models that bimolecular reactions only occur between species whose rovibrational energy follows a Boltzmann (thermal) distribution. That is, any complexes initially formed in non-Boltzmann distributions are assumed to be thermalized by energy-transferring collisions prior to bimolecular reactions. Given the high mole fractions of reactive species, X, in combustion environments, reactive collisions of the complexes with X often occur on the same timescale as energy-transferring collisions - yielding sequences proceeding through non-Boltzmann intermediates across multiple potential energy surfaces. Recent studies have shown that such non-Boltzmann kinetic sequences can have substantial impact on the global reactivity in combustion systems. Simulations of these non-Boltzmann reaction sequences, which can be described in phenomenological kinetic models via chemically termolecular reactions, require that rovibrational excitation from one potential energy surface be carried over to the next. This paper presents an extended theoretical and computational methodology that couples multiple master equations and derives rate constants for phenomenological reactions describing the conversion of thermal reactants to thermal products for use in phenomenological kinetic schemes. The methodology is then implemented using in-house scripts for non-Boltzmann sequences involving $C_2H_3^* + X$ (with $X = O_2$, H, and OH) where $C_2H_3^*$ is formed via H + C_2H_2 association – which were identified as having strong potential for influencing combustion predictions in a recent study. The results reveal that non-Boltzmann reaction sequences for X = O_2 (the primary focus of this paper) significantly alters the total conversion rate from H + C_2H_2 to products and product branching fractions from those of thermal sequential pathways. Furthermore, the present results demonstrate that non-Boltzmann reaction sequences have significant impact - as high as an order of magnitude - on predicted ignition delay times. Similarly, they yield significantly different dependence of ignition delay times with temperature and O₂ mole fraction – yielding signatures that are likely observable experimentally.

© 2020 The Combustion Institute. Published by Elsevier Inc. All rights reserved.

Keywords: Non-Boltzmann; Chemically termolecular reactions; Rovibrationally excited states,

E-mail address: mpburke@columbia.edu (M.P. Burke).

^{*} Corresponding author at: Department of Mechanical Engineering, Columbia University, New York, NY 10027, United States.

1. Introduction

Phenomenological kinetic models - such as those implemented in combustion codes - track only the evolution of thermal species (whose rovibrational energy distribution is described by a Boltzmann distribution at the given temperature). Phenomenological kinetic models must therefore contain phenomenological reactions describing the conversion of thermal sets of reactants to thermal sets of products. Given that many molecular ensembles are initially formed in non-Boltzmann distributions, phenomenological reactions frequently describe complex sequences of multiple reactive and energy-transferring steps. For example, termolecular association reactions (A + B + M = AB)+ M) proceed via a rovibrationally excited intermediate AB* formed via association of A + B followed by energy transfer via collisions with the bath gas M leading to a thermalized AB (AB* + M = AB + M). (Throughout the text, starred species names refer to molecules at a particular energy or molecular ensembles that may or may not be in non-Boltzmann distributions; unstarred species names are reserved for molecular ensembles in a Boltzmann distribution.) To date, kinetic models have generally consisted of only three reaction types: unimolecular, bimolecular, and termolecular association.

Implicit in the presumption of only these three reaction types is the assumption that any rovibrationally excited intermediates AB* are thermalized via energy-transferring collisions prior to undergoing reactive collisions with some reactive species X - such that bimolecular reactions only take place between thermal species (AB + X). However, in many practical reactive environments (especially in combustion), the mole fraction of reactive colliders X (e.g. O₂, H, OH) can be sufficiently high that reactive collisions of rovibrationally excited intermediates AB* with X can occur on similar timescales as energy-transferring collisions with M. Indeed, recent studies [1–7] have demonstrated the impact of non-Boltzmann reaction sequences involving bimolecular reactions of AB* with X on macroscopic reactivity in combustion [4-7] (and atmospheric chemistry [1-3]). For example, Burke and Klippenstein [5] recently demonstrated the impact of reactive collisions of HO₂, formed via H + O_2 association, with X = H, O, and OH - describedphenomenologically as chemically termolecular reactions $(H + O_2 + X)$ – on flame speeds.

As Burke and Klippenstein [5] note, "in principle, almost every bimolecular reaction could arise as a chemically termolecular reaction." Therefore, combinatorically, there are conceivably hundreds to thousands of possible chemically termolecular reactions in typical combustion systems and yet, a priori, it is not straightforward to know which of these many possibilities are sufficiently important to warrant quantification using master equation

calculations. Recently, Barbet et al. [8] introduced an approach to identify and estimate rate constants for each possible chemically termolecular reaction based only on current information about other reactions. Application of this approach within a screening procedure revealed the potential importance of non-Boltzmann kinetic sequences involving reactive collisions of C₂H₃* (formed via H + C_2H_2) with X = H, OH, and O_2 on macroscopic properties of C_2H_2 combustion [8]. Their results [8] revealed both the impact of including $H + C_2H_2$ + X with the thermal product branching ratios and the additional impact of including $H + C_2H_2 + X$ with different product branching ratios. Altogether, these results suggest that the potential impact of such non-Boltzmann sequences $(H + C_2H_2 + X)$ result from their two distinct effects on the kinetics: (1) increased overall rates of conversion of H + C_2H_2 (i.e. via reactive collisions with X consuming $C_2H_3^*$ that would otherwise dissociate back to H + C_2H_2) and (2) altered product branching ratios (i.e. via rovibrational excitation of the $C_2H_3^*$ influencing the products formed in reactive collisions with X).

The potential importance of the identified non-Boltzmann kinetic sequences could be especially significant given that C₂H₂ is one of the major intermediates of hydrocarbon combustion. Consequently, understanding the chemistry of C₂H₂ combustion is important to building hierarchical kinetic models for larger hydrocarbons and, in fact, has been the topic of many previous studies ([9] and the references therein). However, the above-mentioned results from Barbet et al. [8] were based on estimates from an approximate screening procedure intended merely for identifying non-Boltzmann kinetic sequences with strong potential for impact, such that determining the actual role of $H + C_2H_2 + X$ on combustion properties requires improved quantification.

Therefore, for the present study, we performed master equation calculations to quantify rate constants for $H + C_2H_2 + X$ to assess their impact on combustion properties and provide rate constants for use in phenomenological kinetic models. These calculations employ a new methodology for coupling master equations to derive rate constants for phenomenological reactions describing non-Boltzmann sequences spanning multiple potential energy surfaces that bears some similarity to the methodology of Burke et al. [4]. The present methodology goes beyond the earlier methodology [4] by (1) accounting for the additional energy contributed by the rovibrational modes of X and relative translation between AB* and X, (2) accounting for the dependence of the $AB^* + X$ capture rate constants on rovibrational energy of the AB* via a semi-microcanonical approach [1], (3) modifying some aspects of the implementation to facilitate recursive application to an arbitrary number of coupled potential energy surfaces,

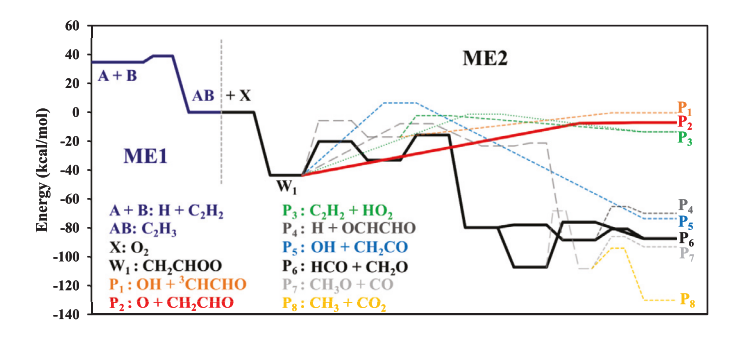


Fig. 1. Potential energy surface [10,11] diagram for the coupled master equation calculations. The major pathways are denoted in solid lines and minor pathways in broken lines. All energies are relative to the ground state of C_2H_3 .

(4) automating the entire workflow from coupled master equations to phenomenological kinetic modeling of combustion.

This methodology was then implemented for $H + C_2H_2 + X$ with $X = O_2$, H, and OH. The discussion and results presented below focus primarily on $X = O_2$, for which we find non-Boltzmann reaction sequences to have a substantial impact, but we also describe calculations for X = H and OH, for which our limited calculations show non-Boltzmann reaction sequences have a lesser effect, in the Supplemental Material.

In particular, we find that reactive collisions of $C_2H_3^*$, formed via $H+C_2H_2$ association, with O_2 both (1) increase the overall rates of conversion of H, C_2H_2 , and O_2 to products and (2) influence the product branching ratios (notably enhancing radical branching). We also find that inclusion of the phenomenological reactions describing such non-Boltzmann kinetic sequences ($H+C_2H_2+O_2$) in combustion kinetic models has a pronounced impact on ignition delay times – of roughly an order of magnitude. The results also indicate pronounced differences in the ignition delay time dependence on temperature and O_2 mole fraction – yielding signatures that are likely observable experimentally.

2. Methodology

Clearly, the "interface" between two reactive systems (e.g. ME1: A + B = AB and ME2: AB + X, as shown in Fig. 1 for A = H, $B = C_2H_2$, and $X = O_2$) is complicated. At the interface between ME1 and ME2, AB^* with rovibrational energy E (group 1) can react with thermally distributed X with energy E' contained in both the rovibrational modes of X and relative translation between X and AB (group 2), where the energy distribution of group 2 follows a Boltzmann distribution with temperature, T. The resultant W_1^* ($C_2H_3O_2^*$ in Fig. 1) would have a rovibrational energy equal to E'' = E + E'. The energy distribution of the produced $W_1^*(E'')$ is then modified through energy-transferring collisions

before further reactions. Ultimately, the rovibrationally excited W_1^* can be thermalized to W_1 , dissociate "backward" to (AB + X)*, or dissociate "forward" along ME2 to form various bimolecular species (P₁-P₈ in Fig. 1). When W₁* dissociates to bimolecular species, the energy in excess of the dissociation threshold is distributed in the rovibrational and relative translational modes of the fragments. And specifically for back dissociation, this energy is partitioned between group 1 and 2. Therefore, the sequence of AB* reacting with X to produce W₁* followed by collisional energy transfer and eventual back dissociation to $(AB + X)^*$, while not consuming AB* on the net, can result in a type association-back-dissociation-driven energy transfer mechanism.

While some methodologies [12,13], utilizing the MESMER code [14], have been shown to exactly satisfy detailed balance [12] (including for the processes involved in the association-back-dissociation energy transfer mechanism), the present methodology, utilizing the MESS code [15], enables calculations of rate constants for phenomenological reactions (from thermal sets of reactants to thermal sets of products) that describe non-Boltzmann kinetic sequences including in situations that require "species merging" [15,16] (which was not a component of the other methodologies [12,13]). In the present methodology, the association-backdissociation energy transfer process is only approximately modeled. In reality, a proper quantification of both typical energy-transferring processes and those involved in the association-back-dissociation mechanism would likely require dynamics calculations, which are not considered here or in [12,13].

The present methodology bears some similarity to the previous methodology of Burke et al. [4], which couples multiple master equations together to track the energy distributions of reacting complexes across multiple potential energy surfaces to calculate rate constants for phenomenological reactions between thermal sets of reactants and thermal sets of products. This previous methodology [4] had also included a novel modification

of the common irreversible sink approach for including bimolecular reactions of AB* and X in ME1 [1–6] that accounted for reversibility (approximately) at the ME1-ME2 interface by treating AB* that reacts with X to form W₁* that back dissociates to have never reacted at all. The present methodology here goes beyond this earlier methodology [4] in the following ways.

First, whereas the earlier methodology [4] neglected the energy contributed by group 2 (the rovibrational modes of X and relative translation between AB* and X) during reaction of AB* + X and energy taken away by group 2 during back dissociation of W_1^* to $(AB + X)^*$, the present methodology accounts for this energy under certain approximations for the energy contained in group 2 upon back dissociation. Namely, the energy contained in group 2 upon back dissociation is assumed to be the same as group 2 contributed to the W₁* energy, such that AB* that reacts with X to form W₁* that dissociates back to AB* can still be considered to have not reacted at all – enabling (1) an approximate treatment of reversibility in AB* + $X = W_1^*$ via a modified irreversible sink rate [4] and (2) a proper treatment of the energy-transferring collisions of the back-dissociated AB* in ME1. However, as discussed above, such a treatment still neglects the above-mentioned association-backdissociation energy transfer mechanism.

Second, whereas the earlier methodology [4] approximated the capture rate constant for $AB^* + X$, $k_{AB^*+X \to W_1^*}(E,T)$, as the thermal capture rate constant for AB + X, $k_{AB^*+X \to W_1^*}(T)$, the present methodology accounts for the energy dependence of $k_{AB^*+X \to W_1^*}(E,T)$ via a semi-microcanonical approach [1]. While this approach [1] assumes that all reactant modes contribute equally to the reaction coordinate (which may not be appropriate particularly for barrierless reactions), its use, when combined with the consideration of energy of group 2, at least allows the thermal rate constants to be correctly reproduced in the low [X] limit.

Third, whereas the earlier methodology [4] employed a single sink in ME1 for the total forward bimolecular reaction rate (which required results from subsequent master equations) and then multiplied this by various branching ratios from multiple subsequent master equations to calculate channel-specific rate constants for thermal reactants, r, to final thermal products, j, the present methodology employs multiple sinks in ME1 that correspond to the channel-specific rate constants to final thermal products, j. We expect that this implementation may facilitate application of the same code to an arbitrary number of master equations through recursion.

Fourth and finally, whereas the earlier methodology [4] was implemented with many manual steps, the present methodology is implemented via an entirely automated workflow from coupled master equations to phenomenological kinetic modeling – enabling tractable calculations over broader ranges of conditions or for different reaction sequences.

2.1. Theoretical approach

Specifically, here, bimolecular reactions AB^* + X are treated using a novel modification of the sink approach [1–6] by including multiple pseudo-first-order sinks in ME1 to simulate product-channel-specific reactions of AB^* + X to thermal products, $j \neq R$, with rates according to

$$\omega_{AB^*(+X)\to j}(E) = k_{AB^*+X\to j}(E;T)[X] \tag{1}$$

where [X] is the concentration of X and $k_{AB^*+X\to j}(E;T)$ is the rate constant for reactions of AB* with rovibrational energy E with X (where group 2 follows a thermal distribution with temperature, T) to ultimately form some set of thermal products, $j=W_j$ or P_j . Note that the exclusion of a sink for j=R, which corresponds to reactions of AB* + X to form W_1^* that ultimately back dissociates, is equivalent to assuming that it never occurred (i.e. in a similar manner to [4]). The rate constant for AB* + X $\rightarrow j$ can then be expressed as

$$k_{AB^*+X\to j}(E; T)$$

$$= \int_0^\infty \{k_{AB^*+X\to W_1^*}(E, E')\alpha_{W_1^*\to j}(E+E') \times f_2(E', T)\}dE'$$
(2)

where $k_{AB^*+X\to W_1^*}(E, E')$ is the capture rate constant for $AB^* + X \rightarrow W_1^*$ for given E and E'; $\alpha_{W_1^* \to i}(E + E')$ is the probability that W_1^* with total rovibrational energy, E + E' = E'', ultimately produces some set of thermal products, j; $f_2(E',$ T) is energy distribution of group 2 at energy E' for the temperature T, which in the situation described above is simply the Boltzmann distribution, $f_2(E', T) = \rho_2(E') \exp(-E'/k_B T)/Q_2(T)$, with $\rho_2(E')$ being the density of states of group 2, k_B being the Boltzmann constant, and $Q_2(T)$ being the partition function for group 2. The density of states of group 2 is the convolution of the density of states for the rovibrational modes of X, $\rho_{X,rovib}$, with that for the relative translation between AB* and X, $\rho_{AB^*-X,trans}$, i.e.

$$\rho_2(E') = \int_0^{E'} \rho_{X,\text{rovib}}(x) \rho_{AB^*-X,\text{trans}}(E'-x) dx \quad (3)$$

Here, $k_{\mathrm{AB^*}+\mathrm{X}\to\mathrm{W}_1^*}(E,E')$ is calculated using the semi-microcanonical approach of Maranzana et al. [1] that assumes that the rate constant depends only on the total energy from groups 1 and 2 combined, E''=E+E', i.e. $k_{\mathrm{AB^*}+\mathrm{X}\to\mathrm{W}_1^*}(E,E')\approx k_{\mathrm{AB^*}+\mathrm{X}\to\mathrm{W}_1^*}(E+E')$, viz.

$$k_{AB^*+X\to W_1^*}(E'') = \frac{1}{h} \frac{N_{12}^{\neq}(E'')}{\rho_{1,2}(E'')}$$
 (4)

where h is Planck's constant; $N_{12}^{\neq}(E'')$ is the number of states for the transition state connecting AB + X and W_1 at energy E''; and $\rho_{1,2}(E'')$ is the convolved density of states of group 1 and 2, i.e.

$$\rho_{1,2}(E'') = \int_0^{E''} \rho_1(E)\rho_2(E'' - E)dE \tag{5}$$

where it may be helpful to note again that E'' - E = E'.

2.2. Implementation

Master equation calculations are performed in PAPR-MESS [15] with PESs for ME1 and ME2 from [10,11]. Given that N_2 and O_2 have similar energy transfer parameters, for simplicity, energy transfer parameters for N_2 [10,17] are used for all the considered mixtures (primarily composed of N_2 and O_2). (Consequently, there are no mixture effects due to different energy transfer parameters among mixture components [18–22].)

In general, in the equations above, $\alpha_{W_1^* \to j}(E'')$ could also encapsulate non-Boltzmann sequences that extend beyond ME2 through treatment of product energy distributions, as in [4,23], or recursion of the present approach. For simplicity, the present calculations do not track energy distributions of non-Boltzmann sequences beyond ME2, which could in particular influence the likelihood that HCO of P₆ promptly dissociates. However, trajectory calculations of Goldsmith et al. [24] suggest that essentially all HCO formed from even thermal $C_2H_3 + O_2$ promptly dissociates, in which case tracking the energy distributions beyond ME2 is not necessary anyway. In this case, $\alpha_{W_1^* \to j}(E'')$ (which is simply the probability that \mathbf{W}_1^* with total rovibrational energy, E'', is stabilized to some thermal complex, W_j, or promptly dissociates to bimolecular species, R or P_i) is directly calculable via MESS [15]. For calculations of $\alpha_{W_i^* \to i}(E'')$ from ME2, for simplicity, all potential wells other than W1 are treated as "merged" species (where they are still considered in the ME but they are not considered among the thermal reactants or products in phenomenological reactions [15,16].)

With the inclusion of pseudo-first-order sinks in ME1 corresponding to each AB* + X \rightarrow *j* (as fictitious dissociation channels) with rates according to Eqs. (1)–(5), pseudo-second-order rate constants, $k_{A+B(+X)\rightarrow j}$, for phenomenological reactions from thermal A + B (i.e. H + C_2H_2) to each set of thermal products *j* can be obtained from MESS [15]. Thereafter, rate constants, $k_{A+B+X\rightarrow j}$, for chemically termolecular reactions of A + B + X (i.e. H + C_2H_2 + O_2) can be obtained by dividing by [X], i.e. $k_{A+B+X\rightarrow j}$ = $k_{A+B(+X)\rightarrow j}$ /[X]. For the present calculations, C_2H_3 is considered to be "merged" [15,16] given its clear non-Boltzmann distributions with high

 $X_{\rm O_2}$ (as found below). (Importantly, when abovementioned procedure is implemented for low $X_{\rm O_2}$ and C_2H_3 is not considered to be "merged", rate constants obtained via ME1 for $C_2H_3 + O_2$ reproduce thermal rate constants obtained directly from ME2.)

(Additional calculations that assess the impact of the above-mentioned association-back-dissociation energy transfer mechanism are presented in the Supplemental Material. The calculations suggest that the additional energy transfer mechanism yields a higher overall rate of conversation of H, C_2H_2 , and O_2 to products and a lower branching ratio to the $O + CH_2CHO$ channel than those presented below. Interestingly, inclusion of these calculated rate constants in kinetic modeling yields similar ignition delay times. Overall, it appears that improved quantification of this process may be worthwhile for improved quantification of $H + C_2H_2 + O_2$.)

2.3. Kinetic modeling

To evaluate the impact of non-Boltzmann reaction sequences on combustion modeling, ignition delay times (IDTs, based on the largest temperature time derivative) under constant-volume, adiabatic conditions are simulated using Cantera 2.4.0 [25]. The model of Glarborg and co-workers [26] is used as the nominal model for IDT simulations (due to its favorable performance in predicting IDTs compared to other models [9]). In the present model variants, $H + C_2H_2 = C_2H_3$ and $C_2H_3 +$ O₂ in the nominal model were replaced with the present calculations. One model variant includes 70% prompt dissociation of HCO in P₆ (to match the nominal model [26]); another includes 100%, which trajectory calculations of Goldsmith et al. [24] indicate is more realistic. (Note that the nominal model [26] employs rate constants calculated via the same ME1 [10] and ME2 [11] files used here, such that the nominal model and model variant with 70% HCO prompt dissociation yield the same results in the low X_{O_2} limit, where C_2H_3 is thermalized prior to bimolecular reactions.)

3. Results and discussion

The computational methods discussed in Section 2, which were automated via in-house scripts, are implemented for the reactive sequence presented in Fig. 1 to evaluate the branching fractions and phenomenological rate constants at various $T/P/X_{\rm O_2}$ conditions. While the results and discussion presented below focus mainly on the non-Boltzmann reaction sequence $H + C_2H_2 + O_2$ at 1 atm, the qualitative trends observed also hold at other pressures (see Supplemental Material).

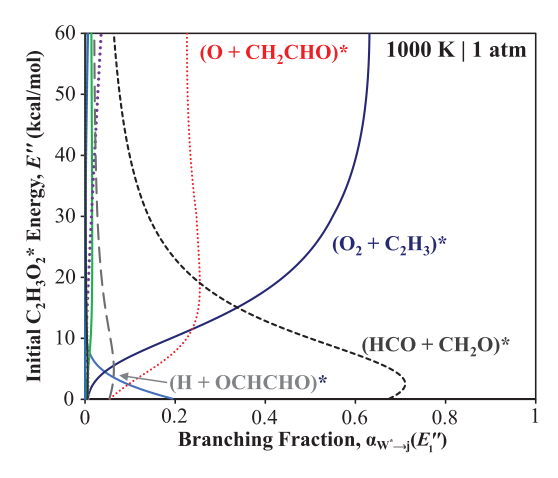


Fig. 2. Branching fractions of $C_2H_3O_2^*$ to various products j, $\alpha_{W_1^* \to j}(E'')$, as a function of initial energy E'' of $C_2H_3O_2^*$ (relative to the ground-state energy of C_2H_3) at 1000 K and 1 atm.

3.1. Microcanonical (energy-resolved) branching fractions

The calculated microcanonical branching fractions of C₂H₃O₂* as a function of nascent energy of $C_2H_3O_2^*$, generated from $C_2H_3^* + O_2$ association, are plotted in Fig. 2 for 1000 K and 1 atm. At low energies, the majority of $C_2H_3O_2^*$ dissociates to (HCO + CH₂O)*, as a result of it being the dominant pathway proceeding via the lowest lying transition states (Fig. 1). At intermediate energies, the branching fraction to $(HCO + CH_2O)^*$ decreases while those to $(C_2H_3 + O_2)^*$ and $(O_2H_3 + O_3)^*$ + CH₂CHO)* increase, such that three sets of products (HCO + CH₂O)*, $(C_2H_3 + O_2)$ * and $(O + CH_2O)$ * $CH_2CHO)^*$ compete for the dissociating $C_2H_3O_2^*$. At high energies, back dissociation becomes the dominant channel for C₂H₃O₂*, followed by dissociation to $(O + CH_2CHO)^*$ due to their (relatively) loose transition states. While the exact values of $\alpha_{W_1^* \to j}(E'')$ are functions of temperature, pressure, and mixture composition, the trends for energy dependence of $\alpha_{W_1^* \to j}(E'')$ observed in Fig. 2 are applicable to a wider range of conditions.

Figure 3 plots the total flux of $C_2H_3^* + O_2$ that dissociates "forward" to various products $j \neq R$ and the fractional fluxes to the two major product channels: (HCO + CH₂O)* and (O + CH₂CHO)*. At sufficiently low X_{O_2} (not shown), where thermalizing collisions greatly outnumber the reactive ones, the energy distribution of reacting $C_2H_3^*$ closely resembles the Boltzmann distribution, yielding $C_2H_3O_2^*$ with an energy distribution concentrated at lower energies; given that $C_2H_3O_2^*$ dissociating to (HCO + CH₂O)* dominates the lowenergy branching of $C_2H_3O_2^*$ (Fig. 2), the majority of the reacting $C_2H_3^* + O_2$ flux forms (HCO +

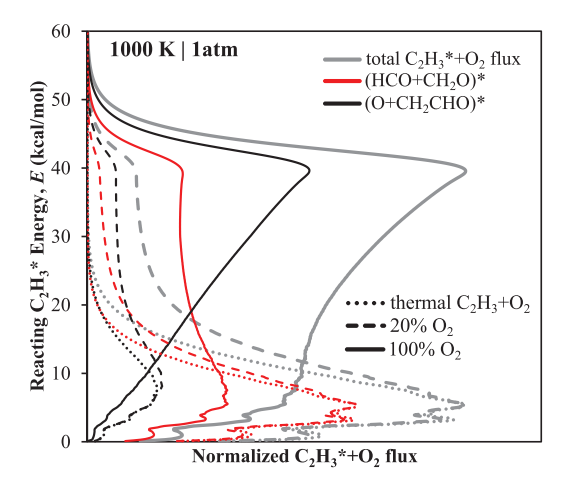


Fig. 3. Total "forward" flux (normalized by peak height) of $C_2H_3^* + O_2$ (gray) and fractional fluxes to the two major channels (black and red) as a function of the rovibrational energy of reacting $C_2H_3^*$ relative to the ground-state energy of C_2H_3 at 1000 K and 1 atm.

CH₂O)* (dotted lines in Fig. 2). As $X_{\rm O_2}$ increases, so does the ratio of reactive to thermalizing collisions; as a result, the energy distribution of reacting C₂H₃ is shifted towards higher energies, yielding C₂H₃O₂* with an energy distribution concentrated at higher energies where (O + CH₂CHO)* is the major product from the "forward" dissociation. Therefore, the fractional flux to (O + CH₂CHO)* becomes more important and essentially dominates as $X_{\rm O_2}$ approaches 100% (dashed and solid lines in Fig. 3).

3.2. Phenomenological rate constants

Figure 4 shows the final branching fractions directly from thermal $H + C_2H_2$ to the two major bimolecular products (O + CH₂CHO)* and (HCO + CH₂O)* at 1 atm and various T/X_{O_2} conditions. The sum of these two channels accounts for over 85% of the total H + C_2H_2 + O_2 flux over the considered conditions. As a result of the energy dependence in Fig. 3, the branching fraction of H $+ C_2H_2 + O_2 = (O + CH_2CHO)^*$ monotonically increases with X_{O_2} while that of H + C_2H_2 + O_2 = $(HCO + CH_2O)^*$ monotonically decreases with X_{O_2} . (For reference, $X_{O_2} = 0$ would correspond to the thermal case.) In addition, since the energy distributions of all reactants shift towards higher energies at higher temperature, the formed $C_2H_3O_2^*$ would also have an energy distribution concentrated at higher energies. This shift results in the positive temperature dependence for the branching fraction of H + C_2H_2 + O_2 = (O + CH_2CHO)*, given that (O + CH₂CHO)* dominates C₂H₃O₂* dissociation at high energies, and the negative temperature dependence for that of $H + C_2H_2 +$ $O_2 = (HCO + CH_2O)^*$. The X_O , dependence tends

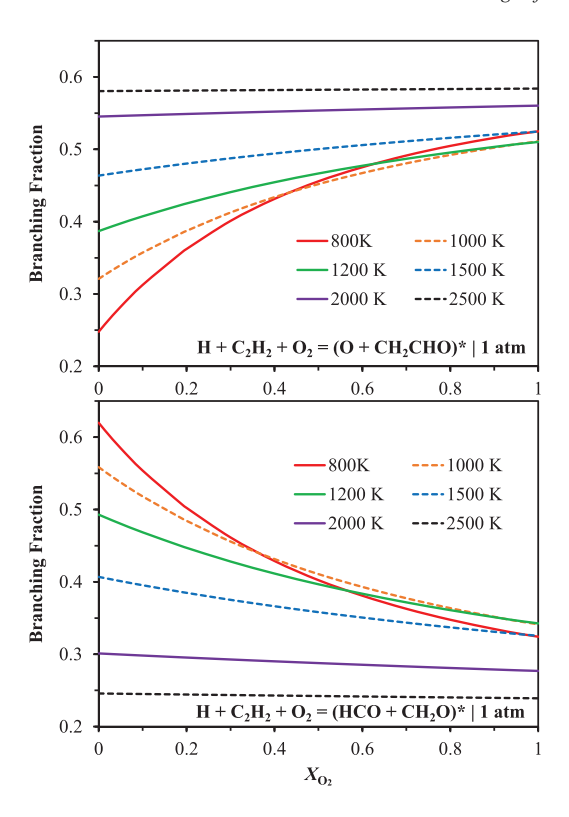


Fig. 4. Branching fractions of $H + C_2H_2 + O_2$ as a function of O_2 mole fraction at 1 atm and various temperatures to the two major products: $H + C_2H_2 + O_2 = (O + CH_2CHO)^*$ (top) and $H + C_2H_2 + O_2 = (HCO + CH_2O)^*$ (bottom).

to be less pronounced at high temperatures, since the $C_2H_3O_2^*$ energy distribution is already concentrated in the region where $\alpha_{C_2H_3O_2^*\to j}(E'')$ only shows weak energy dependence (Fig. 2) such that any shifts in the energy distribution to higher energies with increasing X_{O_2} would only have minor impacts.

Figure 5 presents the calculated rate constants for the total H + C_2H_2 consumption at 1 atm and various T/X_{O_2} conditions, which combined with the information in Fig. 4 gives the channelspecific rate constants from $H + C_2H_2$ (+ O_2) to various thermal products. To evaluate the distinct impact of non-Boltzmann effects on the overall consumption rate of $H + C_2H_2$, Fig. 5 compares pseudo-second-order rate constants for H + C₂H₂ consumption via chemically termolecular reactions (from coupled ME calculations of ME1+ME2 where C2H3 is "merged") and pseudo-second-order rate constants for $H + C_2H_2$ consumption via the thermal sequential pathways (based on rate constants from uncoupled ME calculations of ME1 and ME2 for $H + C_2H_2$ and a quasi-steady-state assumption for C₂H₃ – equiva-

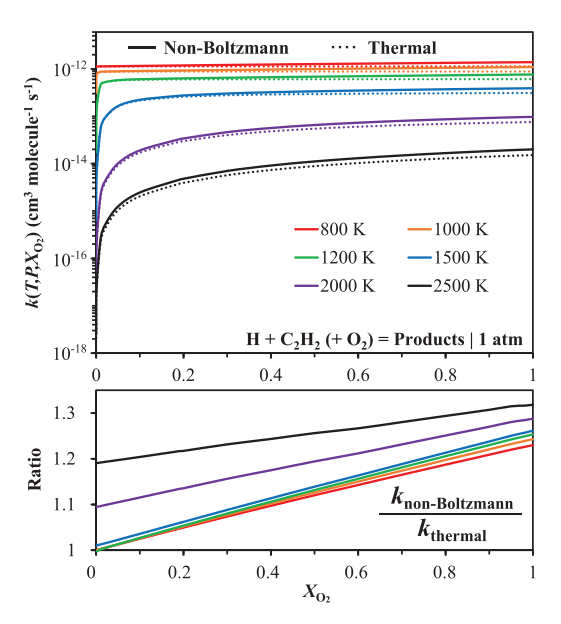


Fig. 5. Pseudo-second-order rate constants for net H + C_2H_2 consumption for thermal sequential pathways and non-Boltzmann sequences (top) and the ratio of rate constants from non-Boltzmann calculations to those assuming thermal C_2H_3 (bottom) at 1 atm for varied T/X_{O_2} . For the thermal case, $k(T, P, X_{O_2}) = (k_1 \cdot k_2[O_2])/(k_{-1} + k_2[O_2])$ is plotted, with thermal rate constants for R1 (H+C₂H₂=C₂H₃) and R2 (C₂H₃+O₂=products).

lent to merging C_2H_3 in the ME calculations). The results indicate that inclusion of reactive collisions of $C_2H_3^*$ serve to increase the overall conversion rate of reactants to products (by up to $\sim 30\%$), because reactive collisions can convert $C_2H_3^*$ complexes (that might otherwise back dissociate to $H+C_2H_2$) to products. These enhancements in the total consumption rate unsurprisingly, are highest at higher temperatures, where the C_2H_3 system is closer to its low-pressure limit regime (where collisions are more rate limiting).

3.3. Implications for combustion kinetic modeling

Combustion simulations are performed to assess the impact of non-Boltzmann $C_2H_3^* + O_2$ on ignition delay times. Simulations are performed using the Glarborg model [26] and modified versions of it that incorporate calculated channel-specific rate constants for $H + C_2H_2 + O_2 \rightarrow$ products. To be consistent with [26] and allow more straightforward comparison, 70% of nascent HCO is assumed to promptly dissociate to H + CO in one scenario. Another (more realistic) scenario where 100% of HCO promptly dissociates is also considered.

Figure 6 shows the predicted IDTs at 1 atm and $\phi = 1.3$ in a C₂H₂/air mixture. Including

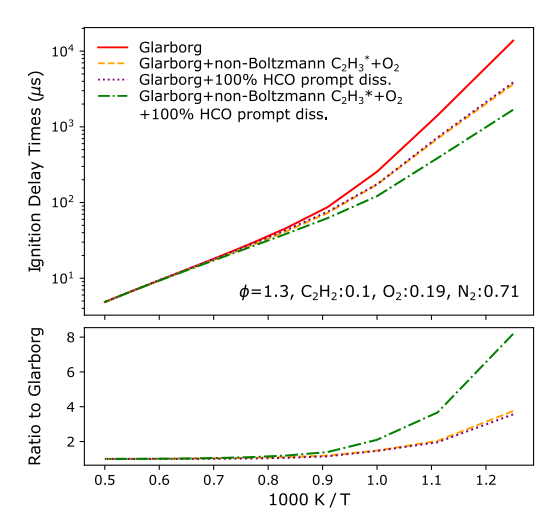


Fig. 6. Ignition delay times for C_2H_2 /air mixtures at 1 atm (top) and ratio of calculated IDTs using Glarborg model [26] to those applying various modifications denoted in legend (bottom).

non-Boltzmann reaction sequences tends to increase the overall system reactivity and reduce the IDTs. As the chain branching reaction $H + C_2H_2$ + $O_2 = O$ + CH_2CHO promotes reactivity, the higher branching fractions to this channel due to non-Boltzmann effects for high X_0 , shorten IDTs (reaching a factor of \sim 4). Non-Boltzmann effects are stronger at lower initial temperatures, where the ratio of chemical activation energy to thermal energy is larger and the enhancement in branching to O + CH2CHO is larger (Fig. 4). Interestingly, if all nascent HCO promptly dissociates, consistent with recent trajectory calculations by Goldsmith et al. [24], the predicted IDTs are a factor of 8 faster than predictions using the nominal Glarborg model. Additional simulations for the X_{O_2} -dependence of IDTs in the Supplemental Material also reveal substantial effects that even yield qualitatively different $X_{\rm O}$, dependence.

Compared to the n-propyl reaction sequence where reactions between non-Boltzmann QOOH* and O_2 were found to be important only at sub-atmospheric pressures (e.g. ~ 30 torr), significant impacts are observed in the current C₂H₃* + O_2 system at higher pressures ($\sim 1-10$ atm). This difference is likely due to the presence of a fairly loose transition state for the radical-radical channel to O + CH_2CHO (Fig. 1), which can compete with the barrierless back dissociation channel to $C_2H_3 + O_2$ even at high energies. Therefore, C₂H₃O₂* at higher energies can dissociate in comparable branching fractions to O + CH₂CHO and $C_2H_3 + O_2$ (Fig. 2) rather than dominantly undergoing back dissociation, which serves to suppress non-Boltzmann effects.

4. Conclusions

A new methodology for calculating rate constants for phenomenological reactions describing non-Boltzmann kinetic sequences spanning multiple potential energy surfaces is presented and applied to H + C_2H_2 + X resulting from $C_2H_3^*$ + X reactions involving C₂H₃* formed via H + $C_2H_2^*$ association. The results for $X = O_2$ reveal significant impacts of non-Boltzmann sequences on total conversion rate from H, C₂H₂, and O₂ to products, product branching fractions from C₂H₃* $+ O_2$, and C_2H_2 ignition delay times. Not only was the impact of $H + C_2H_2 + X$ found to be substantial - as high as an order of magnitude - but also $H + C_2H_2 + X$ manifests in markedly different T and X_{O_2} dependence – yielding signatures that are likely observable experimentally.

Declaration of Competing Interest

None.

Acknowledgments

The authors gratefully acknowledge support from the National Science Foundation Combustion and Fire Systems program (CBET-1706252) and Department of Energy Gas Phase Chemical Physics program (DE-SC0019487) and would also like to thank Stephen Klippenstein and Franklin Goldsmith for sharing the theoretical data for H + C_2H_2 [10] and $C_2H_3 + O_2$ [11].

Supplementary material

Supplementary material associated with this article can be found, in the online version, at doi:10.1016/j.proci.2020.06.385.

References

- A. Maranzana, J.R. Barker, G. Tonachini, *Phys. Chem. Chem. Phys.* 9 (2007) 4129–4141.
- [2] D.R. Glowacki, J. Lockhart, M.A. Blitz, S.J. Klippenstein, M.J. Pilling, S.H. Robertson, P.W. Seakins, *Science* 337 (6098) (2012) 1066–1069.
- [3] M. Pfeifle, M. Olzmann, *Int. J. Chem. Kinet.* 46 (4) (2014) 231–244.
- [4] M.P. Burke, C.F. Goldsmith, Y. Georgievskii, S.J. Klippenstein, *Proc. Combust. Inst.* 35 (1) (2015) 205–213.
- [5] M.P. Burke, S.J. Klippenstein, Nat. Chem. 9 (11) (2017) 1078.
- [6] A.W. Jasper, R. Sivaramakrishnan, S.J. Klippenstein, J. Chem. Phys. 150 (11) (2019) 114112.
- [7] R.E. Cornell, M.C. Barbet, M.P. Burke, Proc. Combust. Inst. (2020) in press, doi:10.1016/j.proci.2020. 06.354.

- [8] M.C. Barbet, K. McCullough, M.P. Burke, Proc. Combust. Inst. 37 (1) (2019) 347–354.
- [9] N. Lokachari, U. Burke, A. Ramalingam, M. Turner, R. Hesse, K.P. Somers, J. Beeckmann, K.A. Heufer, E.L. Petersen, H.J. Curran, *Proc. Combust. Inst.* 37 (1) (2019) 583–591.
- [10] J.A. Miller, S.J. Klippenstein, Phys. Chem. Chem. Phys. 6 (2004) 1192–1202.
- [11] C.F. Goldsmith, L.B. Harding, Y. Georgievskii, J.A. Miller, S.J. Klippenstein, J. Phys. Chem. A 119 (28) (2015) 7766–7779.
- [12] N.J. Green, S.H. Robertson, Chem. Phys. Lett. 605–606 (2014) 44–46.
- [13] R.J. Shannon, S.H. Robertson, M.A. Blitz, P.W. Seakins, Chem. Phys. Lett. 661 (2016) 58–64.
- [14] D.R. Glowacki, C.-H. Liang, C. Morley, M.J. Pilling, S.H. Robertson, J. Phys. Chem. A 116 (38) (2012) 9545–9560.
- [15] Y. Georgievskii, J.A. Miller, M.P. Burke, S.J. Klippenstein, J. Phys. Chem. A 117 (46) (2013) 12146–12154.
- [16] J.A. Miller, S.J. Klippenstein, J. Phys. Chem. A 110 (36) (2006) 10528–10544.
- [17] P. Paul, J. Warnatz, Symp. (Int.) Combust. 27 (1) (1998) 495–504.

- [18] M.P. Burke, R. Song, *Proc. Combust. Inst.* 36 (1) (2017) 245–253.
- [19] L. Lei, M.P. Burke, *J. Phys. Chem. A* 123 (3) (2019a) 631–649.
- [20] L. Lei, M.P. Burke, *Proc. Combust. Inst.* 37 (1) (2019b) 355–362.
- [21] L. Lei, M.P. Burke, *Combust. Flame* 213 (2020) 467–474.
- [22] L. Lei, M.P. Burke, Proc. Combust. Inst (2020) in press, doi:10.1016/j.proci.2020.06.187.
- [23] C.F. Goldsmith, M.P. Burke, Y. Georgievskii, S.J. Klippenstein, *Proc. Combust. Inst.* 35 (1) (2015) 283–290.
- [24] A.D. Danilack, C.F. Goldsmith, *Proc. Combust. Inst.* (2020) in press.
- [25] D.G. Goodwin, R.L. Speth, H.K. Moffat, B.W. Weber, Cantera: An Object-Oriented Software Toolkit for Chemical Kinetics, Thermodynamics, and Transport Processes, 2018.
- [26] J. Gimenez-Lopez, C.T. Rasmussen, H. Hashemi, M.U. Alzueta, Y. Gao, P. Marshall, C.F. Goldsmith, P. Glarborg, *Int. J. Chem. Kinet.* 48 (11) (2016) 724–738.